SARS-CoV-2 causes brain inflammation and induces Lewy body formation in macaques

Ingrid H.C.H.M. Philippens[1,*†], Kinga P. Böszörményi[1†], Jacqueline A. Wubben[1], Zahra C. Fagrouch[1], Nikki van Driel[1], Amber Q. Mayenburg[1], Diana Lozovagia[1], Eva Roos[2], Bernadette Schurink[2], Marianna Bugiani[2], Ronald E. Bontrop[1,3], Jinte Middeldorp[1], Willy M. Bogers[1], Lioe-Fee de Geus-Oei[5,6], Jan A.M. Langermans[1,4], Marieke A. Stammes[1‡], Babs E. Verstrepen[1‡], Ernst J. Verschoor[1‡]

[1] Biomedical Primate Research Centre (BPRC), Lange Kleiweg 161, 2288GJ Rijswijk, The Netherlands

[2] Department of Pathology, Amsterdam UMC, De Boelelaan 1117, 1081HV Amsterdam, The Netherlands

[3] Department of Biology, Theoretical Biology and Bioinformatics, Utrecht University, Padualaan 8, Utrecht, The Netherlands

[4] Department Population Health Sciences, Division of Animals in Science and Society, Faculty of Veterinary Medicine, Utrecht University, Yalelaan 1, 3584CL Utrecht, The Netherlands

[5] Department of Radiology, Leiden University Medical Center, Albinusdreef 2, 2333ZA Leiden, The Netherlands

[6] Biomedical Photonic Imaging Group, University of Twente, Drienerlolaan 5, 7522ND Enschede, The Netherlands

† These authors contributed equally

‡ These authors jointly supervised this work

*Corresponding author. E-mail: philippens@bprc.nl

Keywords: SARS-CoV-2; macaques; brain inflammation; Lewy body formation; neuropathology; PET-CT

Abstract:

SARS-CoV-2 may cause acute respiratory disease, but the infection can also initiate neurological symptoms. Here we show that SARS-CoV-2 infection causes brain inflammation in the macaque model. An increased metabolic activity in the pituitary gland of two macaques was observed by longitudinal positron emission tomography-computed tomography (PET-CT). Post-mortem analysis demonstrated infiltration of T-cells and activated microglia in the brain, and viral RNA was detected in brain tissues from one animal. We observed Lewy bodies in brains of all rhesus macaques. These data emphasize the virus' capability to induce neuropathology in this nonhuman primate model for SARS-CoV-2 infection. As in humans Lewy body formation is an indication for the development of Parkinson's disease, this data represents a warning for potential long-term neurological effects after SARS-CoV-2 infection.

One-Sentence Summar:

SARS-CoV-2 causes brain inflammation and Lewy bodies, a hallmark for Parkinson, after an asymptomatic infection in macaques.

52 **Report**

53 Severe acute respiratory syndrome coronavirus 2 (SARS-CoV-2) causes a multi-system
54 inflammatory disease syndrome, COVID-19 (*1*). Although SARS-CoV-2 predominantly affects
55 the respiratory organs, over 30% of the hospitalized COVID-19 patients also suffer from
56 neurological manifestations, including loss of smell or taste, delirium, diminished consciousness,
57 epilepsy, and psychosis (*2-5*). Besides these general neurological symptoms, some patients
58 additionally endure Parkinsonism (*6-8*). The mechanisms behind this process are poorly
59 understood. Neurological symptoms may be triggered by infection of the brain tissue, or indirectly,
60 via virus-induced immune cell activation (*9*). In humans a direct link between brain inflammation
61 and the presence of SARS-CoV-2 RNA has not yet been established (*10*), and thus, formal proof
62 that central nervous system (CNS)-related symptoms of COVID-19 are directly caused by the
63 infection, or indirectly due to overactivation of the immune system, is lacking. Additionally, the
64 long-term effects on the CNS after a mild to moderate SARS-CoV-2 infection, likely the vast
65 majority of human cases, are unknown, and post-mortem brain samples from these individuals are
66 not expected to become available for research in the near future. Controlled infection studies in a
67 standardized experimental setting are crucial to investigate SARS-CoV-2-induced brain pathology
68 (*11*). To address this issue, a study was performed in two macaques species, rhesus macaques
69 (*Macaca mulatta*) and cynomolgus macaques (*Macaca fascicularis)* (Table 1), both well-accepted
70 animal models for COVID-19 (*12*). Four male rhesus and four male cynomolgus macaques were
71 inoculated with 10^6 $TCID_{50}$ of SARS-CoV-2 strain BetaCoV/BavPat1/2020 via a combined
72 intratracheal and intranasal route (*13, 14*). Following infection, SARS-CoV-2 genomic material
73 was detected in tracheal and nasal swabs up to ten days, and based on clinical signs and thorax
74 CTs, all animals showed mild to moderate disease symptoms (*13, 15*). We initiated weekly ^{18}F-FDG

75 PET-CTs of the animals' brains of all macaques when the virus became undetectable in nasal and
76 tracheal swabs. The uptake of tracer renders a marker for metabolic activity. Two of four
77 cynomolgus macaques (C1 and C2), displayed an increased uptake of ^{18}F-FDG in the pituitary gland
78 at multiple time points. In animal C1, an increased uptake of ^{18}F-FDG in the pituitary gland was
79 seen at days 30 and 36 post-infection (Fig. 1). In animal C2, increased metabolic activity was
80 already visible at day 8 and continued through day 35 when the final scan was obtained (Table S1).
81 In humans and macaques, the volume of the pituitary gland is small, and under physiological
82 conditions its metabolic activity is comparable to the background level of the entire brain (*16, 17*).
83 The ^{18}F-FDG uptake of the pituitary gland may even be underestimated due to the partial-volume-
84 effects that affect the emission signal recovery (*16*). Because pituitary gland tissue expresses
85 angiotensin-converting enzyme 2 (ACE2)(*18*), the increased ^{18}F-FDG uptake may be a direct effect
86 of the infection or an indirect effect due to either a (reversible) hypophysitis, or transient
87 hypothalamic-pituitary dysfunction. Yet, hypocortisolism has never been documented in patients
88 with active COVID-19 (*19*).
89 To further investigate the consequences of SARS-CoV-2-infection on macaque brain tissue, the
90 animals were euthanized 5-6 weeks after experimental infection. Sections of the whole brain were
91 systematically collected for further examination. As several regions of the brain express the SARS-
92 CoV-2 receptor ACE2, and inflammation was found in the human brain (*10, 20, 21*), we used
93 various immunological markers for innate and adaptive immune activation to investigate for signs
94 of immune activation, and also explored the localization of virus particles (Fig. 2 and Table 2).
95 Viral RNA was detected by real-time quantitative polymerase chain reaction (RT-qPCR) in
96 multiple brain areas of the right hemisphere of cynomolgus macaque C3 (Fig. 2). More precisely,
97 cerebellum (1.48×10^5 RNA genome equivalents (GE)/gram), medial motor cortex (2.09×10^5

98 GE/gram), sensory cortex ($2.07x10^5$ GE/gram) and frontal basal cortex ($8.29x10^4$ GE/gram), as well
99 as hippocampus ($1.24x10^5$ GE/gram), hypothalamus ($1.05x10^6$ GE/gram), and globus pallidus
100 ($5.45x10^4$ GE/gram) all tested positive in the RT-qPCR. No viral RNA was detected in samples
101 collected from the pituitary gland or olfactory bulb, substantia nigra, medulla oblongata, pons,
102 nucleus caudatus, and putamen. Subgenomic viral RNA analysis did not show evidence for active
103 virus replication in the brains at the time-point of euthanasia. Additionally, SARS-CoV-2 antigen
104 was not detectable by immunohistochemistry the brains of all macaques.
105 The brains of all SARS-CoV-2-infected macaques showed evidence of inflammation. Presence of
106 T-cells was visualized by CD3 staining in intraparenchymal brain tissue, suggesting the infiltration
107 of T-cells that passed the blood-brain barrier after SARS-CoV-2 infection (Fig.3A, top panel).
108 Additionally, activation of microglia cells in different areas of the brain, including the olfactory
109 bulb and pituitary gland, was confirmed by Mamu-DR staining (upregulation of MHC class II
110 expression) (Fig. 3A, middle panel). However, nodule formation, which is a measure for severity
111 of activation, was rarely present (Table 2). No B-lymphocytic infiltration was found as evidenced
112 by lack of CD20 staining (not shown). Hematoxylin and eosin (HE) staining did not show any
113 abnormalities in the brain tissue of the virus-exposed macaques, including the absence of
114 ischemic/necrotic lesions. For comparison, post-mortem brain tissues from two healthy, age-
115 matched macaques of each species were used as controls (Table 1), none of the four control animals
116 displayed obvious signs of immune activation (T-cells and microglia) were observed.
117 Brain tissues were screened for α-synuclein deposits, known as Lewy bodies, by
118 immunohistochemistry. In humans, Lewy body formation is linked to the development of
119 Parkinson's disease or Lewy body dementia (*22, 23*). It has been hypothesized that certain

120 neurotropic viruses, including MERS and SARS coronaviruses, can trigger formation of Lewy
121 bodies and cause Parkinsonism (*24-29*).
122 The formation of intracellular Lewy bodies was clearly shown in the midbrain region of the caudate
123 nucleus of all infected rhesus macaques (Table 2, Fig. 3B), and in one aged cynomolgus macaque
124 (C4), while Lewy bodies were absent in the brains of all four control animals. The data provide
125 evidence for SARS-CoV-2-driven inflammation in the brain of macaques. In humans,
126 neuropathology has been described in moribund COVID-19 patients, but we report of SARS-CoV-
127 2-related brain involvement in macaques without displaying overt clinical signs. In general,
128 macaque models for SARS-CoV-2 infection typically represent mild to moderate COVID-19
129 symptoms on the CT scan, as compared to humans (*12, 14, 30*). Detection of viral RNA in the brain
130 of an animal demonstrates the virus' neuroinvasive capability. This matches a recent study
131 describing neuroinvasion in mouse brains and in human brain organoids (*31*).
132 How exactly SARS-CoV-2 caused widespread brain inflammation and induced Lewy body
133 formation remains unknown. Viruses can enter the brain via different pathways. In this study,
134 infiltration of T-cells was found perivascular and in the brain parenchyma, which indicates that the
135 blood-brain barrier integrity may have been disturbed, offering the virus the opportunity to enter
136 the brain. Alternatively, we hypothesize that SARS-CoV-2 gained access to the brain via neuronal
137 pathways, such as the retrograde and anterograde neuronal transport through infected motor or
138 sensory neurons (*32*), and can have entered the pituitary gland via binding to the ACE2 receptor
139 protein expressed on its cell surfaces (*18, 33*). Such neural connection also exists between the
140 olfactory bulb and the nasal mucosa (*34*), and the loss of taste and smell, a characteristic of COVID-
141 19, can thus be explained by nasal infection and subsequent inflammation in the olfactory bulb.
142 Such a scenario is in line with the finding that in all the SARS-CoV-2-exposed macaques, immune

system activation in the olfactory bulb was evidenced by the presence of T-cells and/or activated microglia.

Neuronal transport can also explain why some COVID-19 patients develop Parkinson's disease-like symptoms. Viruses can also, via retrograde transport in parasympathic motor neurons of the nervus vagus to the medulla, pons, and midbrain, reach the substantia nigra in the midbrain (*26, 35*). Notably, the α-synuclein inclusions were found in the ventral midbrain region of the animals. In humans, these inclusions of accumulated misfolded proteins are associated with Parkinson's disease or Lewy body dementia (*36*).

There is a growing concern that symptomatic COVID-19 patients may suffer from long-term consequences (*9, 37*). In this light the finding of Lewy bodies in brains of infected macaques without overt clinical signs is intriguing. They are considered a hallmark for the development of Parkinson's disease, or Lewy body dementia. More confirmation is required, but the observations in the translational macaque models for COVID-19 (*12-14, 38, 39*) can be regarded as a serious warning as they may be predictive for COVID-19-related dementia cases in humans in the future, even after an asymptomatic infection or mild disease process.

References

1. V. Coronaviridae Study Group of the International Committee on Taxonomy of, The species Severe acute respiratory syndrome-related coronavirus: classifying 2019-nCoV and naming it SARS-CoV-2. *Nat Microbiol* **5**, 536-544 (2020).
2. L. Mao, H. Jin, M. Wang, Y. Hu, S. Chen, Q. He, J. Chang, C. Hong, Y. Zhou, D. Wang, X. Miao, Y. Li, B. Hu, Neurologic Manifestations of Hospitalized Patients With Coronavirus Disease 2019 in Wuhan, China. *JAMA Neurol* **77**, 683-690 (2020).
3. R. W. Paterson, R. L. Brown, L. Benjamin, R. Nortley, S. Wiethoff, T. Bharucha, D. L. Jayaseelan, G. Kumar, R. E. Raftopoulos, L. Zambreanu, V. Vivekanandam, A. Khoo, R. Geraldes, K. Chinthapalli, E. Boyd, H. Tuzlali, G. Price, G. Christofi, J. Morrow, P. McNamara, B. McLoughlin, S. T. Lim, P. R. Mehta, V. Levee, S. Keddie, W. Yong, S. A. Trip, A. J. M. Foulkes, G. Hotton, T. D. Miller, A. D. Everitt, C. Carswell, N. W. S. Davies, M. Yoong, D. Attwell, J. Sreedharan, E. Silber, J. M. Schott, A. Chandratheva, R. J. Perry, R. Simister, A. Checkley, N. Longley, S. F. Farmer, F. Carletti, C. Houlihan, M.

173 Thom, M. P. Lunn, J. Spillane, R. Howard, A. Vincent, D. J. Werring, C. Hoskote, H. R.
174 Jager, H. Manji, M. S. Zandi, U. C. L. Q. S. N. H. f. Neurology, C.-S. G. Neurosurgery,
175 The emerging spectrum of COVID-19 neurology: clinical, radiological and laboratory
176 findings. *Brain*, (2020).
177 4. M. Fotuhi, A. Mian, S. Meysami, C. A. Raji, Neurobiology of COVID-19. *J Alzheimers*
178 *Dis* **76**, 3-19 (2020).
179 5. A. Giacomelli, L. Pezzati, F. Conti, D. Bernacchia, M. Siano, L. Oreni, S. Rusconi, C.
180 Gervasoni, A. L. Ridolfo, G. Rizzardini, S. Antinori, M. Galli, Self-reported Olfactory
181 and Taste Disorders in Patients With Severe Acute Respiratory Coronavirus 2 Infection:
182 A Cross-sectional Study. *Clin Infect Dis* **71**, 889-890 (2020).
183 6. M. E. Cohen, R. Eichel, B. Steiner-Birmanns, A. Janah, M. Ioshpa, R. Bar-Shalom, J. J.
184 Paul, H. Gaber, V. Skrahina, N. M. Bornstein, G. Yahalom, A case of probable
185 Parkinson's disease after SARS-CoV-2 infection. *Lancet Neurol* **19**, 804-805 (2020).
186 7. I. Faber, P. R. P. Brandao, F. Menegatti, D. D. de Carvalho Bispo, F. B. Maluf, F.
187 Cardoso, Coronavirus Disease 2019 and Parkinsonism: A Non-post-encephalitic Case.
188 *Mov Disord* **35**, 1721-1722 (2020).
189 8. A. Mendez-Guerrero, M. I. Laespada-Garcia, A. Gomez-Grande, M. Ruiz-Ortiz, V. A.
190 Blanco-Palmero, F. J. Azcarate-Diaz, P. Rabano-Suarez, E. Alvarez-Torres, C. P. de
191 Fuenmayor-Fernandez de la Hoz, D. Vega Perez, R. Rodriguez-Montalban, A. Perez-
192 Rivilla, J. Sayas Catalan, A. Ramos-Gonzalez, J. Gonzalez de la Aleja, Acute
193 hypokinetic-rigid syndrome following SARS-CoV-2 infection. *Neurology* **95**, e2109-
194 e2118 (2020).
195 9. M. T. Heneka, D. Golenbock, E. Latz, D. Morgan, R. Brown, Immediate and long-term
196 consequences of COVID-19 infections for the development of neurological disease.
197 *Alzheimers Res Ther* **12**, 69 (2020).
198 10. B. Schurink, E. Roos, T. Radonic, E. Barbe, C. S. C. Bouman, H. H. de Boer, G. J. de
199 Bree, E. B. Bulle, E. M. Aronica, S. Florquin, J. Fronczek, L. M. A. Heunks, M. D. de
200 Jong, L. Guo, R. du Long, R. Lutter, P. C. G. Molenaar, E. A. Neefjes-Borst, H. W. M.
201 Niessen, C. J. M. van Noesel, J. Roelofs, E. J. Snijder, E. C. Soer, J. Verheij, A. P. J.
202 Vlaar, W. Vos, N. N. van der Wel, A. C. van der Wal, P. van der Valk, M. Bugiani, Viral
203 presence and immunopathology in patients with lethal COVID-19: a prospective autopsy
204 cohort study. *Lancet Microbe* **1**, e290-e299 (2020).
205 11. S. Natoli, V. Oliveira, P. Calabresi, L. F. Maia, A. Pisani, Does SARS-Cov-2 invade the
206 brain? Translational lessons from animal models. *Eur J Neurol* **27**, 1764-1773 (2020).
207 12. C. Munoz-Fontela, W. E. Dowling, S. G. P. Funnell, P. S. Gsell, A. X. Riveros-Balta, R.
208 A. Albrecht, H. Andersen, R. S. Baric, M. W. Carroll, M. Cavaleri, C. Qin, I. Crozier, K.
209 Dallmeier, L. de Waal, E. de Wit, L. Delang, E. Dohm, W. P. Duprex, D. Falzarano, C. L.
210 Finch, M. B. Frieman, B. S. Graham, L. E. Gralinski, K. Guilfoyle, B. L. Haagmans, G.
211 A. Hamilton, A. L. Hartman, S. Herfst, S. J. F. Kaptein, W. B. Klimstra, I. Knezevic, P.
212 R. Krause, J. H. Kuhn, R. Le Grand, M. G. Lewis, W. C. Liu, P. Maisonnasse, A. K.
213 McElroy, V. Munster, N. Oreshkova, A. L. Rasmussen, J. Rocha-Pereira, B. Rockx, E.
214 Rodriguez, T. F. Rogers, F. J. Salguero, M. Schotsaert, K. J. Stittelaar, H. J. Thibaut, C. T.
215 Tseng, J. Vergara-Alert, M. Beer, T. Brasel, J. F. W. Chan, A. Garcia-Sastre, J. Neyts, S.
216 Perlman, D. S. Reed, J. A. Richt, C. J. Roy, J. Segales, S. S. Vasan, A. M. Henao-
217 Restrepo, D. H. Barouch, Animal models for COVID-19. *Nature* **586**, 509-515 (2020).

13. K. P. Böszörményi, M. A. Stammes, Z. C. Fagrouch, G. Kiemenyi-Kayere, H. Niphuis, D. Mortier, N. van Driel, I. Nieuwenhuis, E. Zuiderwijk-Sick, L. Meijer, P. Mooij, E. J. Remarque, G. Koopman, A. C. R. Hoste, P. Sastre, B. L. Haagmans, R. E. Bontrop, J. A. M. Langermans, W. M. Bogers, E. J. Verschoor, B. E. Verstrepen, Comparison of SARS-CoV-2 infection in two non-human primate species: rhesus and cynomolgus macaques. *bioRxiv*, 11.05.369413 (2020).
14. B. Rockx, T. Kuiken, S. Herfst, T. Bestebroer, M. M. Lamers, B. B. Oude Munnink, D. de Meulder, G. van Amerongen, J. van den Brand, N. M. A. Okba, D. Schipper, P. van Run, L. Leijten, R. Sikkema, E. Verschoor, B. Verstrepen, W. Bogers, J. Langermans, C. Drosten, M. Fentener van Vlissingen, R. Fouchier, R. de Swart, M. Koopmans, B. L. Haagmans, Comparative pathogenesis of COVID-19, MERS, and SARS in a nonhuman primate model. *Science* **368**, 1012-1015 (2020).
15. F. Pan, T. Ye, P. Sun, S. Gui, B. Liang, L. Li, D. Zheng, J. Wang, R. L. Hesketh, L. Yang, C. Zheng, Time Course of Lung Changes at Chest CT during Recovery from Coronavirus Disease 2019 (COVID-19). *Radiology* **295**, 715-721 (2020).
16. M. Meyer, G. Allenbach, M. Nicod Lalonde, N. Schaefer, J. O. Prior, S. Gnesin, Increased (18)F-FDG signal recovery from small physiological structures in digital PET/CT and application to the pituitary gland. *Sci Rep* **10**, 368 (2020).
17. S. Goutal, N. Tournier, M. Guillermier, N. Van Camp, O. Barret, M. Gaudin, M. Bottlaender, P. Hantraye, S. Lavisse, Comparative test-retest variability of outcome parameters derived from brain [18F]FDG PET studies in non-human primates. *PLoS One* **15**, e0240228 (2020).
18. R. Pal, M. Banerjee, COVID-19 and the endocrine system: exploring the unexplored. *J Endocrinol Invest* **43**, 1027-1031 (2020).
19. R. Pal, COVID-19, hypothalamo-pituitary-adrenal axis and clinical implications. *Endocrine*, (2020).
20. I. Hamming, W. Timens, M. L. Bulthuis, A. T. Lely, G. Navis, H. van Goor, Tissue distribution of ACE2 protein, the functional receptor for SARS coronavirus. A first step in understanding SARS pathogenesis. *J Pathol* **203**, 631-637 (2004).
21. M. Hoffmann, H. Kleine-Weber, S. Schroeder, N. Kruger, T. Herrler, S. Erichsen, T. S. Schiergens, G. Herrler, N. H. Wu, A. Nitsche, M. A. Muller, C. Drosten, S. Pohlmann, SARS-CoV-2 Cell Entry Depends on ACE2 and TMPRSS2 and Is Blocked by a Clinically Proven Protease Inhibitor. *Cell* **181**, 271-280 e278 (2020).
22. Z. Walker, K. L. Possin, B. F. Boeve, D. Aarsland, Lewy body dementias. *Lancet* **386**, 1683-1697 (2015).
23. M. Sezgin, B. Bilgic, S. Tinaz, M. Emre, Parkinson's Disease Dementia and Lewy Body Disease. *Semin Neurol* **39**, 274-282 (2019).
24. T. Yamada, Viral etiology of Parkinson's disease: Focus on influenza A virus. *Parkinsonism Relat Disord* **2**, 113-121 (1996).
25. R. L. Doty, The olfactory vector hypothesis of neurodegenerative disease: is it viable? *Ann Neurol* **63**, 7-15 (2008).
26. I. Mori, Viremic attack explains the dual-hit theory of Parkinson's disease. *Med Hypotheses* **101**, 33-36 (2017).
27. E. M. Gatto, J. Fernandez Boccazzi, COVID-19 and neurodegeneration: what can we learn from the past? *Eur J Neurol* **27**, e45 (2020).

28. A. Y. Vittor, M. Long, P. Chakrabarty, L. Aycock, V. Kollu, S. T. DeKosky, West Nile Virus-Induced Neurologic Sequelae-Relationship to Neurodegenerative Cascades and Dementias. *Curr Trop Med Rep* **7**, 25-36 (2020).
29. S. Ait Wahmane, A. Achbani, Z. Ouhaz, M. Elatiqi, A. Belmouden, M. Nejmeddine, The Possible Protective Role of alpha-Synuclein Against Severe Acute Respiratory Syndrome Coronavirus 2 Infections in Patients With Parkinson's Disease. *Mov Disord* **35**, 1293-1294 (2020).
30. D. K. Singh, B. Singh, S. R. Ganatra, M. Gazi, J. Cole, R. Thippeshappa, K. J. Alfson, E. Clemmons, O. Gonzalez, R. Escobedo, T. H. Lee, A. Chatterjee, Y. Goez-Gazi, R. Sharan, M. Gough, C. Alvarez, A. Blakley, J. Ferdin, C. Bartley, H. Staples, L. Parodi, J. Callery, A. Mannino, B. Klaffke, P. Escareno, R. N. Platt, 2nd, V. Hodara, J. Scordo, S. Gautam, A. G. Vilanova, A. Olmo-Fontanez, A. Schami, A. Oyejide, D. K. Ajithdoss, R. Copin, A. Baum, C. Kyratsous, X. Alvarez, M. Ahmed, B. Rosa, A. Goodroe, J. Dutton, S. Hall-Ursone, P. A. Frost, A. K. Voges, C. N. Ross, K. Sayers, C. Chen, C. Hallam, S. A. Khader, M. Mitreva, T. J. C. Anderson, L. Martinez-Sobrido, J. L. Patterson, J. Turner, J. B. Torrelles, E. J. Dick, Jr., K. Brasky, L. S. Schlesinger, L. D. Giavedoni, R. Carrion, Jr., D. Kaushal, Responses to acute infection with SARS-CoV-2 in the lungs of rhesus macaques, baboons and marmosets. *Nat Microbiol* **6**, 73-86 (2021).
31. E. Song, C. Zhang, B. Israelow, A. Lu-Culligan, A. V. Prado, S. Skriabine, P. Lu, O. E. Weizman, F. Liu, Y. Dai, K. Szigeti-Buck, Y. Yasumoto, G. Wang, C. Castaldi, J. Heltke, E. Ng, J. Wheeler, M. M. Alfajaro, E. Levavasseur, B. Fontes, N. G. Ravindra, D. Van Dijk, S. Mane, M. Gunel, A. Ring, S. A. J. Kazmi, K. Zhang, C. B. Wilen, T. L. Horvath, I. Plu, S. Haik, J. L. Thomas, A. Louvi, S. F. Farhadian, A. Huttner, D. Seilhean, N. Renier, K. Bilguvar, A. Iwasaki, Neuroinvasion of SARS-CoV-2 in human and mouse brain. *J Exp Med* **218**, (2021).
32. P. A. Swanson, 2nd, D. B. McGavern, Viral diseases of the central nervous system. *Curr Opin Virol* **11**, 44-54 (2015).
33. E. Lazartigues, M. M. F. Qadir, F. Mauvais-Jarvis, Endocrine Significance of SARS-CoV-2's Reliance on ACE2. *Endocrinology* **161**, (2020).
34. J. Meinhardt, J. Radke, C. Dittmayer, J. Franz, C. Thomas, R. Mothes, M. Laue, J. Schneider, S. Brünink, S. Greuel, M. Lehmann, O. Hassan, T. Aschman, E. Schumann, R. L. Chua, C. Conrad, R. Eils, W. Stenzel, M. Windgassen, L. Rößler, H.-H. Goebel, H. R. Gelderblom, H. Martin, A. Nitsche, W. J. Schulz-Schaeffer, S. Hakroush, M. S. Winkler, B. Tampe, F. Scheibe, P. Körtvélyessy, D. Reinhold, B. Siegmund, A. A. Kühl, S. Elezkurtaj, D. Horst, L. Oesterhelweg, M. Tsokos, B. Ingold-Heppner, C. Stadelmann, C. Drosten, V. M. Corman, H. Radbruch, F. L. Heppner, Olfactory transmucosal SARS-CoV-2 invasion as a port of central nervous system entry in individuals with COVID-19. *Nature Neuroscience*, (2020).
35. C. H. Hawkes, K. Del Tredici, H. Braak, Parkinson's disease: a dual-hit hypothesis. *Neuropathol Appl Neurobiol* **33**, 599-614 (2007).
36. J. P. Taylor, J. Hardy, K. H. Fischbeck, Toxic proteins in neurodegenerative disease. *Science* **296**, 1991-1995 (2002).
37. M. Marshall, The lasting misery of coronavirus long-haulers. *Nature* **585**, 339-341 (2020).
38. H. Zheng, H. Li, L. Guo, Y. Liang, J. Li, X. Wang, Y. Hu, L. Wang, Y. Liao, F. Yang, Y. Li, S. Fan, D. Li, P. Cui, Q. Wang, H. Shi, Y. Chen, Z. Yang, J. Yang, D. Shen, W. Cun,

X. Zhou, X. Dong, Y. Wang, Y. Chen, Q. Dai, W. Jin, Z. He, Q. Li, L. Liu, Virulence and pathogenesis of SARS-CoV-2 infection in rhesus macaques: A nonhuman primate model of COVID-19 progression. *PLoS Pathog* **16**, e1008949 (2020).

39. V. J. Munster, F. Feldmann, B. N. Williamson, N. van Doremalen, L. Perez-Perez, J. Schulz, K. Meade-White, A. Okumura, J. Callison, B. Brumbaugh, V. A. Avanzato, R. Rosenke, P. W. Hanley, G. Saturday, D. Scott, E. R. Fischer, E. de Wit, Respiratory disease in rhesus macaques inoculated with SARS-CoV-2. *Nature* **585**, 268-272 (2020).
40. M. A. Stammes, J. Bakker, R. A. W. Vervenne, D. G. M. Zijlmans, L. van Geest, M. P. M. Vierboom, J. A. M. Langermans, F. A. W. Verreck, Recommendations for Standardizing Thorax PET–CT in Non-Human Primates by Recent Experience from Macaque Studies. *Animals* **11**, 204 (2021).
41. V. M. Corman, O. Landt, M. Kaiser, R. Molenkamp, A. Meijer, D. K. Chu, T. Bleicker, S. Brunink, J. Schneider, M. L. Schmidt, D. G. Mulders, B. L. Haagmans, B. van der Veer, S. van den Brink, L. Wijsman, G. Goderski, J. L. Romette, J. Ellis, M. Zambon, M. Peiris, H. Goossens, C. Reusken, M. P. Koopmans, C. Drosten, Detection of 2019 novel coronavirus (2019-nCoV) by real-time RT-PCR. *Euro Surveill* **25**, (2020).
42. R. Wolfel, V. M. Corman, W. Guggemos, M. Seilmaier, S. Zange, M. A. Muller, D. Niemeyer, T. C. Jones, P. Vollmar, C. Rothe, M. Hoelscher, T. Bleicker, S. Brunink, J. Schneider, R. Ehmann, K. Zwirglmaier, C. Drosten, C. Wendtner, Virological assessment of hospitalized patients with COVID-2019. *Nature* **581**, 465-469 (2020).
43. G. Paxinos, X. F. Huang, M. Petrides, A. Toga, *The Rhesus Monkey Brain: in Stereotaxic Coordinates*. (Elsevier Science Publishing Co Inc, San Diego, Ca., ed. 2nd, 2008), pp. 416.

Acknowledgements

We want to thank Francisca van Hassel for assistance with editing of figures, Yolanda Kap for reviewing the manuscript, Wim Vos for the excellent histology, and the Animal Science Department of the BPRC, the veterinarians and animal caretakers for all the experimental support.

Funding

This study was supported by funding from the Biomedical Primate Research Centre. KPB was supported by the European Union's Marie Skłodowska-Curie Innovative Training Network HONOURs; grant agreement no. 721367.

Author contributions

Conceptualization: IHCHMP, EJV, MAS, BEV

Data curation: MAS, BEV, IHCHMP

Formal Analysis: MAS, IHCHMP, BEV

Funding acquisition: EJV

Investigation: JAW, ZCF, NvD, AQM, DL

Methodology: MAS, MB, BS, IHCHMP

Project administration: EJV, BEV

Resources: REB

Supervision: IHCHMP, MAS, BEV, EJV

Validation: MB, ER, L-FG-O,

Writing – original draft: IHCHMP, KPB

Writing – review & editing: MAS, EJV, BEV, JAML, REB, JM, WMB,

Competing interests:

The authors declare that they have no competing interests.

Data and materials availability:

All data are available in the main text or the supplementary materials. Correspondence and request for materials should be addressed to IHCHMP (philippens@bprc.nl).

363 **Table 1: Animals featuring in this study**

Macaque species	Monkey ID	Infected Y/N	Age (Year)	Body weight[#] (kg)	Sex M/F
Rhesus	R1	Y	6	8.2	M
Rhesus	R2	Y	5	7.9	M
Rhesus	R3	Y	5	7.8	M
Rhesus	R4	Y	5	8.7	M
Rhesus	control R5	N	5	8.5	M
Rhesus	control R6	N	6	5.1	F
Cynomolgus	C1	Y	4	5.7	M
Cynomolgus	C2	Y	4	3.3	M
Cynomolgus	C3	Y	4	4.9	M
Cynomolgus	C4	Y	16	9.7	M
Cynomolgus	control C5	N	5	5.3	M
Cynomolgus	control C6	N	7	5.1	M

364 [#]at start of study

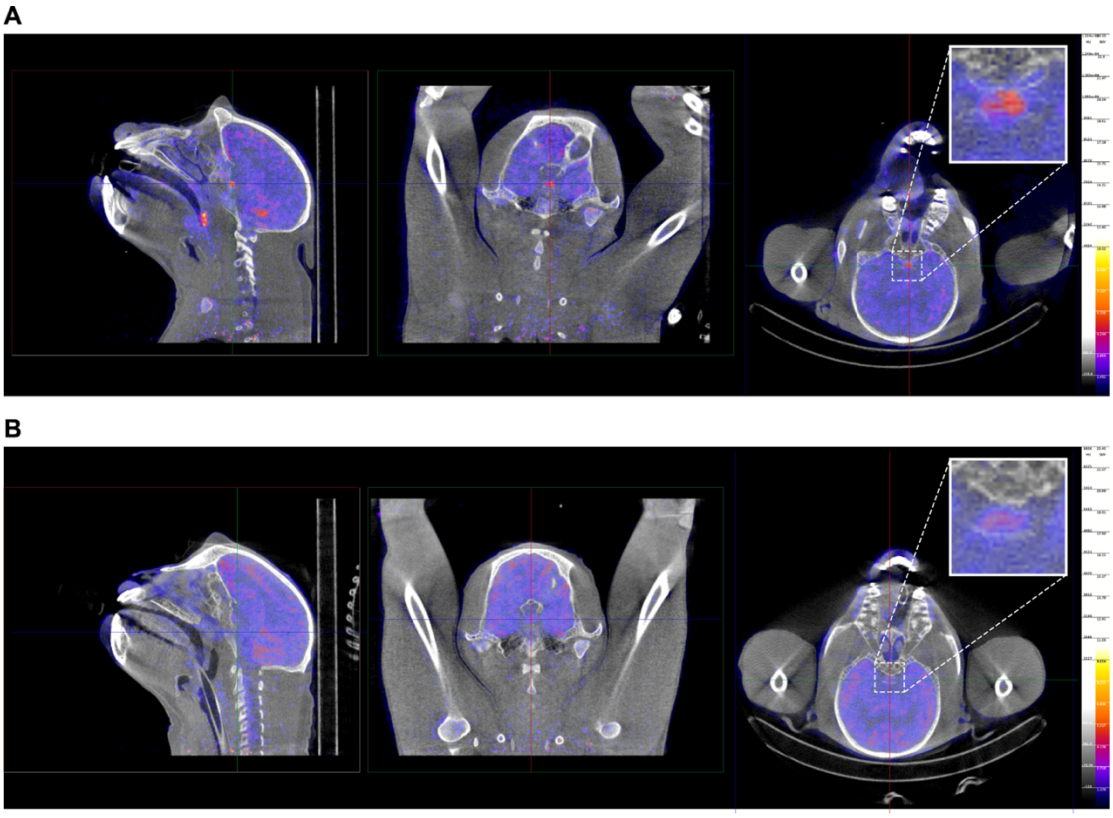

Fig. 1. ^{18}F-FDG PET-CT image of a SARS-CoV-2 infected cynomolgus macaque (C1). Representative images of cynomolgus macaque C1 (A) on day 29, and a healthy control animal (B) are shown. The pituitary gland is indicated by the cross-hairs in all three directions and is boxed (right pictures). Similar window-level settings are applied for all sections. The pituitary gland-brain ratio of animal C1 was calculated with both the mean and peak standard uptake value (SUV); for the SUV_{mean} this ratio was 1.9, and for the SUV_{peak} 1.3. The average values calculated from a group of non-infected control animals (n=6) were 1.1 (std 0.3) for the SUV_{mean}, and 0.6 (std 0.1) for the SUV_{peak} ratio. The uptake values of the brain, defined as background, were similar with SUV_{mean} values of 2.2 and 1.9 for the SARS-CoV-2-infected animals and the non-infected controls, respectively. After the relevant corrections for attenuation, scatter and decay, our results are indeed indicative for pituitary hypermetabolism after SARS-CoV-2 infection in animals C1 and C2.

377

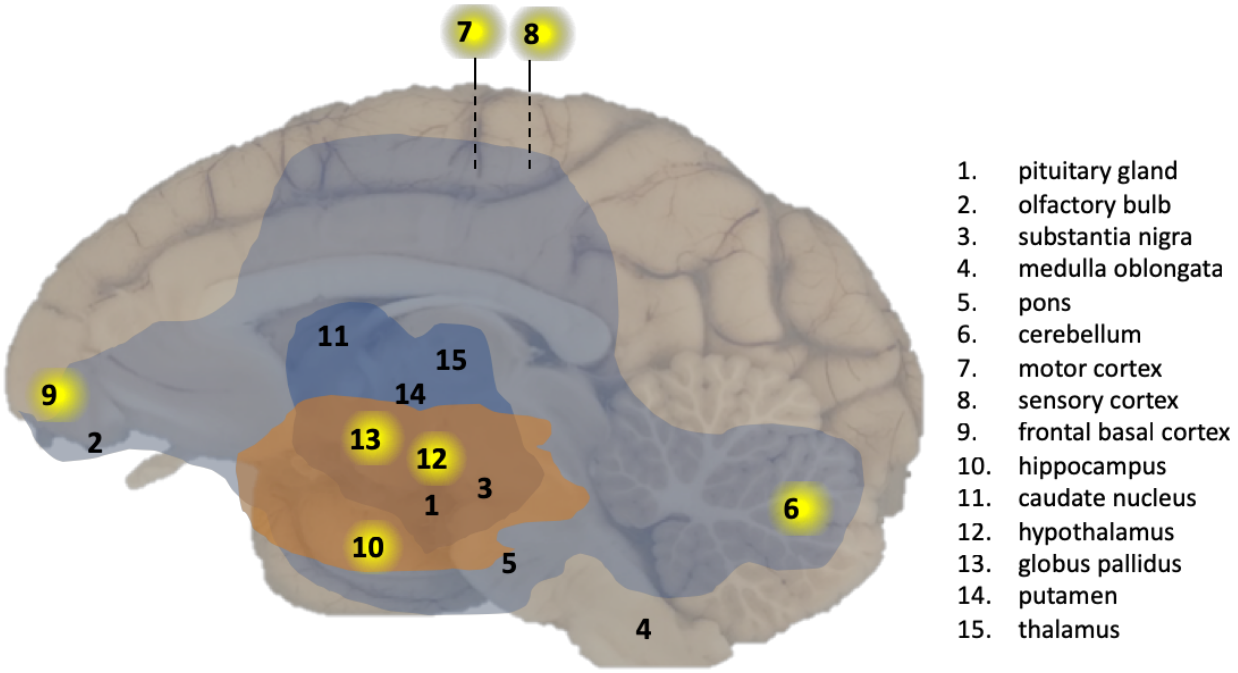

378

379 **Fig. 2. Overview of CNS effects by SARS-CoV-2 exposure in a macaque brain.** Presence of
380 viral RNA was investigated in multiple regions of the brain as indicated by the numbers. Viral
381 RNA-positive regions in cynomolgus macaque C3 are indicated by a yellow background. The
382 analysed brain regions are indicated with a number. Brain areas with T-cells (CD3+) and activated
383 microglia (Mamu-DR+) are shown in light blue (mild expression) and dark blue (moderate
384 expression), respectively. Brain areas with Lewy bodies (α-synuclein+) are shown in orange.

385

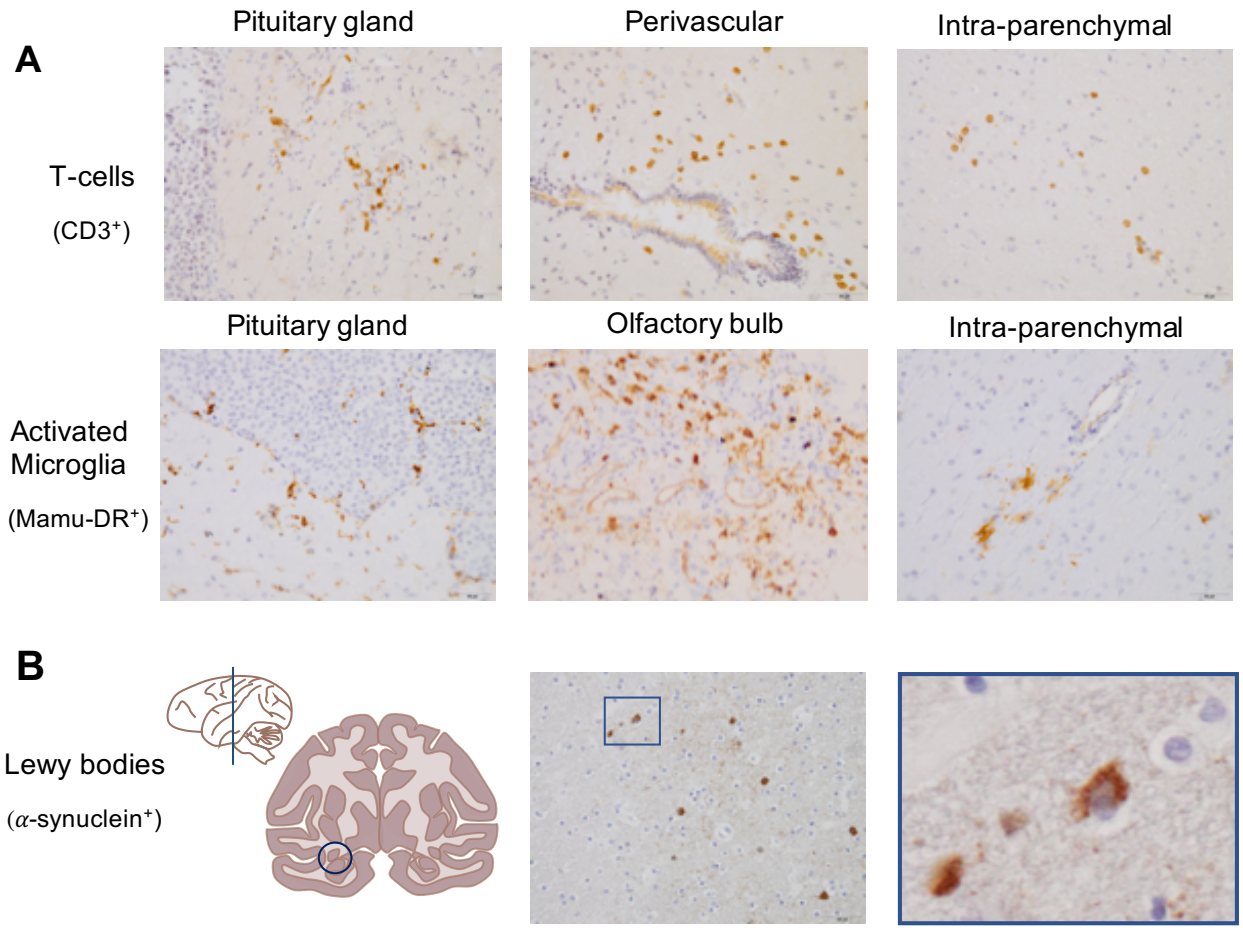

386

387 **Fig. 3. SARS-CoV-2 causes brain inflammation and Lewy body formationin brains of**
388 **macaques.** Immunohistochemical stainings of macaque brain tissues. **A, t**op panel: T-cells (CD3+)
389 in the pituitary gland (left), perivascular (middle) and in the brain parenchyma (right) from a rhesus
390 macaque (20x). **A,** middle panel: activated microglia (Mamu-DR+) in the pituitary gland (left),
391 olfactory bulb (middle) and in the brain parenchyma (right) from a cynomolgus macaque (20x). **B,**
392 bottom panel: Lewy bodies (α-synuclein +) were found next to the hippocampus next to the caudate
393 nucleus indicated with a circle (left) in the coronal section of one hemisphere (anterior-posterior
394 0), presence of Lewy bodies in a SARS-CoV-2-infected rhesus macaque (20x) (middle), a
395 magnified image (40x) of the square in the left image (right).

396

397 **Table 2**: **Histological findings.**

Marker		Brain area	Rhesus				Cynomolgus				Controls			
			R1	R2	R3	R4	C1	C2	C3	C4	R5	R6	C5	C6
T-cells (CD3+)	intra-parenchymal	pituitary gland												
		olfactory bulb												
		front brain												
		dorsal												
		ventral												
		cerebellum												
	perivasculair	pituitary gland												
		olfactory bulb												
		front brain												
		dorsal												
		ventral												
		cerebellum												
	nodules	pituitary gland												
		olfactory bulb												
		front brain												
		dorsal												
		ventral												
		cerebellum												
	meninges	pituitary gland												
		olfactory bulb												
		front brain												
		dorsal												
		ventral												
		cerebellum												
Activated microglia (Mamu-DR+)	presence	pituitary gland												
		olfactory bulb												
		front brain												
		dorsal												
		ventral												
		cerebellum												
	morphology: ramified/ amoeboid	pituitary gland												
		olfactory bulb												
		front brain												
		dorsal												
		ventral												
		cerebellum												
	nodules	pituitary gland												
		olfactory bulb												
		front brain												
		dorsal												
		ventral												
		cerebellum												
	meninges	pituitary gland												
		olfactory bulb												
		front brain												
		dorsal												
		ventral												
		cerebellum												
Lewy bodies (α-synuclein+)	inclusions	ventral midbrain												

398

399

400 Table 2 outlines the presence of 1) T-cells (CD3+ cells) in the brain tissue (intraparenchymal),

401 around blood vessels (perivascular), in group formation (nodules), or in the meninges, 2) activated

402 microglia (Mamu-DR+ cells) in different parts of the brain, the morphology as a measure for the
403 severity of activation (ramified or amoeboid), in group formation (nodules) or in the meninges, 3)
404 α-synuclein/Lewy bodies (α-synuclein + cells with inclusions) in the ventral midbrain region of
405 the caudate nucleus. The last column shows the absence of most of these markers in the control
406 animals. Light grey: mild observation; dark grey: moderate observation (including amoeboid
407 microglia cells); black: moderate to severe observation of these markers.
408
409
410
411
412
413
414
415
416
417
418
419
420
421
422
423
424
425
426
427
428
429
430

Supplementary Materials for

SARS-CoV-2 causes brain inflammation and induces Lewy body formation in macaques

Ingrid H.C.H.M. Philippens[1,*,†], Kinga P. Böszörményi[1,†], Jacqueline A. Wubben[1], Zahra C. Fagrouch[1], Nikki van Driel[1], Amber Q. Mayenburg[1], Diana Lozovagia[1], Eva Roos[2], Bernadette Schurink[2], Marianna Bugiani[2], Ronald E. Bontrop[1,3], Jinte Middeldorp[1], Willy M. Bogers[1], Lioe-Fee de Geus-Oei[5,6], Jan A.M. Langermans[1,4], Marieke A. Stammes[1,‡], Babs E. Verstrepen[1,‡], Ernst J. Verschoor[1,‡]

[1] Biomedical Primate Research Centre (BPRC), Lange Kleiweg 161, 2288GJ Rijswijk, The Netherlands

[2] Department of Pathology, Amsterdam UMC, De Boelelaan 1117, 1081HV Amsterdam, The Netherlands

[3] Department of Biology, Theoretical Biology and Bioinformatics, Utrecht University, Padualaan 8, Utrecht, The Netherlands

[4] Department Population Health Sciences, Division of Animals in Science and Society, Faculty of Veterinary Medicine, Utrecht University, Yalelaan 1, 3584CL Utrecht, The Netherlands

[5] Department of Radiology, Leiden University Medical Center, Albinusdreef 2, 2333ZA Leiden, The Netherlands

[6] Biomedical Photonic Imaging Group, University of Twente, Drienerlolaan 5, 7522ND Enschede, The Netherlands

† These authors contributed equally

‡ These authors jointly supervised this work

*Corresponding author. E-mail: philippens@bprc.nl

This file includes: Materials and Methods, Table S1

462 **MATERIALS AND METHODS**

463

464 **Animals and SARS-CoV-2 exposure**

465 Four cynomolgus macaques (*Macaca fascicularis*) and four Indian-origin rhesus macaques
466 (*Macaca mulatta*) (Table 1) were selected for this study. All macaques were mature, outbred
467 animals, purpose-bred and socially housed at the BPRC. The animals were in good physical health
468 with normal baseline biochemical and hematological values. All were pair-housed with a socially
469 compatible cage-mate. The animals were offered a daily diet consisting of monkey food pellets
470 (Ssniff, Soest, Germany) supplemented with vegetables and fruit. Enrichment was provided daily
471 in the form of pieces of wood, mirrors, food puzzles, and a variety of other homemade or
472 commercially available enrichment products. Drinking water was available *ad libitum* via an
473 automatic system. Animal Care staff provided daily visual health checks before infection, and
474 twice-daily after infection. The animals were monitored for appetite, general behavior, and stool
475 consistency. All possible precautions were taken to ensure the welfare and to avoid any discomfort
476 to the animals. All experimental interventions (intratracheal and intranasal infection, swabs, blood
477 samplings, and PET-CTs) were performed under anesthesia. The research protocol was approved
478 by an independent animal ethics committee (DEC), as well as BPRC's institutional animal welfare
479 body (IvD).

480 On day 0, all animals were exposed to a dose of 10^5 $TCID_{50}$ of SARS-CoV-2 (strain
481 BetaCOV/BavPat1/2020), diluted in 5 ml phosphate-buffered saline (PBS). The virus was
482 inoculated via a combination of the intratracheal route (4.5 ml) and intranasal route (0.25 ml per
483 nostril). For the histological examination brains from naive control macaques from the same age
484 were obtained from the BPRC biobank, two cynomolgus, and two rhesus macaques.

485

486 **Positron Emission Tomography – Computed Tomography**

487 Positron Emission Tomography (PET)-computed tomography (CT) data were acquired on multiple
488 time points post-infection using a MultiScan Large Field of View Extreme Resolution Research
489 Imager (LFER) 150 PET-CT (Mediso Medical Imaging Systems Ltd., Budapest, Hungary) as
490 described before(*40*). Animals were fasted overnight (glucose level > 8.5 mmol/l). The animals
491 were sedated with ketamine (10 mg/kg ketamine hydrochloride (Alfasan Nederland BV, Woerden,
492 The Netherlands)) combined with medetomidine hydrochloride (0.05 mg/kg (Sedastart; AST
493 Farma B.V., Oudewater, The Netherlands)) to induce sedation and muscle relaxation, both applied
494 intramuscularly (IM). The animals were positioned head first supine (HFS) with the arms up. The
495 scans were acquired under mechanical ventilation in combination with a forced breathing pattern.
496 For anesthetic maintenance, a minimum alveolar concentration of isoflurane (iso-MAC) of around
497 0,80%-1.00% was used. The body temperature of the animal was maintained by using the Bair
498 Hugger (3M™, St Paul, MN, USA) supplied with 43˚C airflow. Typically, around 100 MBq of ^{18}F-
499 FDG was applied intravenously (GE Healthcare, Leiderdorp, NL). Thirty minutes after injection
500 the plateau in tracer activity uptake is reached, subsequently a PET of 15 minutes was acquired.
501 After the scan, upon return to their home cage, atipamezole hydrochloride (Sedastop, ASTFarma
502 B.V., Oudewater, NL, 5 mg/ml, 0.25 mg/kg) was administrated IM to antagonize medetomidine.
503 Afterward the emission data was iteratively reconstructed (OSEM3D, 8 iterations, and 9 subsets)
504 into a single frame PET image normalized and corrected for attenuation, scatter, and random
505 coincidences using a reference CT and corrected for radioactive decay. The analysis was performed
506 in VivoQuant 4.5 (Invicro, Boston, USA). Based on repeatability parameters for correct
507 interpretation of the results, a standardized uptake value (SUV) ratio was used for robustness(*17,*
508 *40*). An increased uptake, and pituitary gland hypermetabolism is defined as a SUV_{mean} ratio above

509 1.5 for the pituitary gland over the surrounding brain in combination with a SUV_{peak} ratio above
510 background levels (>1.0). A group of non-infected control rhesus macaques (n=6) were used to
511 calculate average background uptake of ^{18}F-FDG.
512
513 **Brain tissue collection**
514 Five weeks after virus exposure the macaques were euthanized and the brains were collected for
515 further examination. The right hemisphere was used for RT-qPCR analysis and the left hemisphere
516 was fixed in formalin for histology. Fifteen different regions were collected from the right
517 hemisphere for RT-qPCR analysis: 1) part of the pituitary gland, 2) the olfactory bulb, 3) substantia
518 nigra, 4) medulla oblongata, 5) pons, 6) anterior part of the cerebellum, 7) motor cortex medial, 8)
519 sensory cortex, 9) frontal basal cortex, 10) hippocampus, 11) caudate nucleus, 12) hypothalamus,
520 13) globus pallidus, 14) putamen, and 15) thalamus. For the preparation of paraffin-embedded
521 sections of the formalin-fixed left hemisphere, the cerebrum and cerebellum were dissected in 3-4
522 mm parts on the anterior-posterior axis. Pituitary gland and olfactory bulb were also embedded.
523 From each part, sections (4 μm) were prepared for different staining methods.
524 Immunohistochemistry stains were used for T-cells (CD3), B-cells (CD20), activated microglia
525 (Mamu-DR), Lewy bodies (α-synuclein ab), and for SARS-CoV-2. Hematoxyline-eosine (HE)
526 staining was used for general morphology.
527
528 **Viral RNA detection in brain tissue**
529 Brain tissue samples were weighed and placed in gentleMACS M tubes (30 mg in 100 μl PBS) and
530 treated using a gentleMACS Tissue Dissociator (protein01 program)(Miltenyi Biotec B.V., Leiden,
531 The Netherlands). Next, the homogenized tissue was centrifuged, and 100 μl supernatant was used

532 for RNA isolation. Viral RNA was isolated from using a QIAamp Viral RNA Mini kit (Qiagen
533 Benelux BV, Venlo, The Netherlands) following the manufacturer's instructions. Viral RNA was
534 reverse-transcribed to cDNA using a Transcriptor First Strand cDNA Synthesis kit (Roche
535 Diagnostics BV, Almere, The Netherlands). Viral RNA was quantified by RT-qPCR specific for
536 RdRp gene of SARS-CoV-2, as described by Corman *et al.*(*41*). The lower detection limit of the
537 RT-qPCR was 3.6 viral RNA copies per reaction. Viral sub-genomic RNA was detected essentially
538 as described by Wölfel *et al.*(*42*). For both assays, RNA standard curves were generated by *in vitro*
539 transcription of the target regions.
540
541 **Tissue preparation for histology**
542 The left hemisphere of the brains, part of the pituitary gland, and one olfactory bulb were fixed in
543 formalin for 24 hours and thereafter stored in buffered PBS. Preserved brains were cryoprotected
544 in 30% w/v sucrose in PBS. The cerebrum was dissected in 12 different parts cut anterior-posterior
545 axis at +10, +8, +5, +1, -3, -6, -8, -11, -14, -18, -22 from Bregma(*43*), the cerebellum and pons
546 were cut in 4 parts. These part were embedded in paraffin. From the eight brain parts in which viral
547 RNA was detected by RT-qPCR, strips of brain sections were sliced into 12-series of 4 μm sections
548 for different stains. These parts included the frontal cortex, midbrain parts, cerebellum, pituitary
549 gland, and olfactory bulb. Sections were stained with virus antibody staining for virus detection
550 and immunohistochemistry for immune reaction such as T-cell staining (CD3), B-cell staining
551 (CD20), MHC-II cell staining (HLA-DR). Mirror sections were analyzed with a HE staining for
552 brain morphology.
553
554 **Immunohistochemistry**

555 The optimal concentration was determined for each antibody: CD3 (polyclonal rabbit – anti-human
556 CD3 IgG, cat. no. A045201-2, Agilent Technologies), 1:60; CD20 (monoclonal mouse – anti-
557 human CD20 IgG2a, clone L26, cat. no. M075501-2, Agilent Technologies), 1:800; Mamu-DR
558 (monoclonal mouse – anti-human HLA-DR/DQ- IgG1, clone CR3/43, cat. no. M077501-2, Agilent
559 Technologies), 1:150. For antigen retrieval, a steamer was used. Antigen Retrieval solution: IHC-
560 TEK epitope retrieval solution, ready to use (catno IW-1100, IHC world). All incubation steps
561 were at room temperature unless mentioned otherwise. Additionally, hematoxylin was used as a
562 counterstaining in all protocols. After a dehydration sequence, the slides were mounted in Malinol.
563 The counting of cells was performed in a blind matter.

564

565 *CD3 and CD20 staining*

566 The slides were deparaffinized by putting the slides sequentially in xylene, 100% ethanol, 96%
567 ethanol, 70% ethanol, and PBS. Subsequently, an epitope antigen retrieval was executed in a
568 steamer for 1h. After cooling down, the slides were placed in cuvettes (Sequenza cover plate system
569 productnr 36107 Ted Pella inc.). Endogenous peroxidase (PO) activity was blocked by the PO
570 blocking solution from DAKO (S2023) for 15 minutes. After a washing step (PBS with 0.05%
571 Tween) Avidin was added from the DAKO kit (X0590) for 10 minutes. Thereafter, another
572 washing step and biotin was added from the same DAKO kit (10 min) for blocking endogenous
573 biotine. After washing a blocking step was executed for 20 minutes (PBS with 0.1% BSA and 1%
574 normal human serum, NHS). The primary antibody was added (diluted in 0.1% BSA in PBS) and
575 the slices were left overnight at 4°C. After washing a secondary antibody (Rabbit-anti-mouse IgG
576 biotinylated (E0354), Agilent Technologies; 1:200 diluted in PBS + 1% BSA + 1% NHS) was
577 added and, after washing, the slides were incubated with Vectastain ABC-peroxidase (ABC-PO,

578 from Vector Laboratories; PK-4000; diluted 1:100 in PBS) for 30 minutes. After washing, 3,3'-
579 diaminobenzidine (DAB) with 0.02% H_20_2 was added to visualize the antigen-antibody binding (20
580 min).
581
582 *Mamu-DR staining*
583 The EnVision™ staining kit (G|2 Double-stain System, Rabbit/Mouse, DAB+/Permanent RED
584 code K5361; Agilent technologies, Dako DK) was used for the immunohistochemical stain of
585 Mamu-DR. The slides were deparaffinized by putting them sequentially in xylene, 100% ethanol,
586 96% ethanol, 70% ethanol, and PBS?. Subsequently, an epitope antigen retrieval was executed and
587 the slides were put in a steamer for 1h. The cooled down slides were placed in cuvettes and the
588 endogenous peroxidase activity was blocked by the envision kit. The slides were washed and
589 thereafter a blocking step was used consisting of 1% NHS + 1% BSA + 0.2% triton x100 in PBS
590 for 10 minutes. Subsequently, the primary antibody was added (diluted in 0.1% BSA/PBS) for 30
591 minutes. Thereafter a washing step was implemented and the EnVision™ polymer/HRP (secondary
592 antibody) was added for 10 minutes. Polymer HRP was added for 10 minutes followed by a
593 washing step. Thereafter DAB+ was added for 15 minutes to visualize the antigen-antibody
594 binding.
595
596 *α-Synuclein staining*
597 The slides were deparaffinized by immersing them sequentially in xylene, 100% ethanol, 96%
598 ethanol, 70% ethanol, and PBS. Subsequently, an epitope antigen retrieval was executed by putting
599 the slides for 15 minutes in Formic acid (100%) diluted 1:10 in demineralized water. After 2
600 washing steps in PBS with 0,05% Tween, the slides were placed in cuvettes (Sequenza cover plate

601 system product no. 36107 Ted Pella inc.). Endogenous PO activity was blocked by the PO blocking
602 solution from DAKO (S2023) for 20 minutes. After washing (PBS with 0.05% Tween), avidin was
603 added from the DAKO kit (X0590) for 10 minutes. Then, after another washing step, biotin was
604 added from the same DAKO kit (10 min) for blocking of endogenous biotine. After washing, a
605 blocking step was executed for 30 minutes (PBS with 0.1% BSA and 1% NHS and 0.02% Triton-
606 X100). The primary antibody, α-synuclein clone 4D6 (Biolegend SIG-39720), was added (diluted
607 in 0.1% BSA in PBS) and the slides were left overnight at 4°C. After washing, a secondary antibody
608 (rabbit anti-mouse IgG Biotinylated (E0354), Agilent Technologies; 1:200 diluted in PBS + 1%
609 BSA) was added for 30 minutes and the slides were incubated with Vectastain ABC-PO kit from
610 Vector Laboraties (PK-4000; diluted 1:100 in PBS) for 30 minutes. After a final washing step,
611 DAB with 0.02% H_20_2 was added to visualize the Antigen-antibody binding (20 min).
612
613 *SARS-CoV-2 staining*
614 The Roche Optiview DAB IHC kit was used in a Ventana Benchmark Ultra (Roche, Basel
615 Switzerland) immunostainer to immunohistochemically stain SARS-CoV-2. Two monoclonal
616 antibodies of ThermoFisher raised to SARS-CoV-2 Nucleocapsid (clone B46F, catno MA1-7404,
617 and E16C, catno. MA1-7403) were validated on formaldehyde-fixed and paraffin-embedded
618 SARS-CoV-2 and mock-infected Vero E6 cells(*10*), as well as lung tissue sections of human
619 SARS-CoV-2 patients. The clone E16C was superior to B46F and was further used in this study.
620 Antigen retrieval took place with cell conditioning 1 (CC1 , Ventana Medical Systems) (pH 8,5)
621 for 24 minutes at 100°C, 1/5.000 diluted. Thereafter, incubation took place with the primary
622 antibody for 48 minutes at 36°C followed by standard Optiview detection/visualization with DAB
623 and Copper. After immunohistochemical staining, the sections were dehydrated with grades of

624 ethanol and cleared with xylene. All sections were mounted with TissueTek® coverslipping film
625 (Sakura Finetek Europe B.V., Alphen aan den Rijn, The Netherlands).
626
627
628 **Table S1: Quantitative PET-CT analysis of the macaque brains**
629 The standardized uptake values (SUVs) of animals C1 and C2 are represented together with the
630 SUVs of six non-infected control rhesus macaques. Of these animals the average and peak uptake
631 are determined for the pituitary gland, and the brain minus the pituitary gland. By dividing these
632 the pituitary gland/brain ratio is calculated. For the SUVmean values above 1.0 are defined as
633 slightly increased (light grey) and increased (dark grey) when equal or above 1.5. For the SUVpeak
634 values above 1.0 are demarcated as slightly increased and above 1.2 as increased.

C1	**SUVmean**					**SUVpeak**				
Tissue/day	*D8/10*	*D16/17*	*D22/23*	*D28/29*	*D35/36*	*D8/10*	*D16/17*	*D22/23*	*D28/29*	*D35/36*
Pituitary gland	3.1	2.5	2.5	3.5	3.9	5.3	3.9	4.1	6.1	6.4
Brain	2.2	1.9	2.4	1.9	2.6	5.0	4.6	4.7	4.6	4.6
Ratio	1.4	1.3	1.0	1.9	1.5	1.1	0.8	0.9	1.3	1.4
C2	**SUVmean**					**SUVpeak**				
Tissue/day	*D8/10*	*D16/17*	*D22/23*	*D28/29*	*D35/36*	*D8/10*	*D16/17*	*D22/23*	*D28/29*	*D35/36*
Pituitary gland	3.1	2.6	2.7	3.8	3.2	7.1	6.3	4.5	6.5	6.1
Brain	2.0	1.8	2.1	2.2	2.1	5.1	3.6	3.8	5.0	3.8
Ratio	1.5	1.5	1.3	1.7	1.5	1.4	1.8	1.2	1.3	1.6

635

Controls	**SUVmean**						**SUVpeak**					
Tissue/ animal	*NHP1*	*NHP2*	*NHP3*	*NHP4*	*NHP5*	*NHP6*	*NHP1*	*NHP2*	*NHP3*	*NHP4*	*NHP5*	*NHP6*
Pituitary gland	2.3	2.6	2.1	2.7	1.3	1.3	3.3	3.7	2.9	3.9	1.9	1.6
Brain	2.3	2.0	1.9	1.9	1.5	1.8	5.6	6.1	4.9	3.9	3.7	3.5
Ratio	1.0	1.3	1.1	1.4	0.9	0.7	0.6	0.6	0.6	1.0	0.5	0.5

636

637